ELSEVIER

Electroencephalography and clinical Neurophysiology 105 (1997) 345–351

Topographic mapping of trans-cranial magnetic stimulation data on surface rendered MR images of the brain

K.D. Singh[a,*], S. Hamdy[b], Q. Aziz[b], D.G. Thompson[b]

[a]*Department of Psychology, Royal Holloway College, University of London, Egham, Surrey, UK*
[b]*Department of Medicine, Hope Hospital, Eccles Old Road, Manchester, UK*

Accepted for publication: 30 January 1997

Abstract

We present a method for the coregistration and topographic mapping of trans-cranial magnetic stimulation (TCMS) data on surface rendered images of the cortex, derived from Magnetic Resonance Images (MRI). We describe the TCMS procedure and the methods used to locate the TCM stimulation sites in the MRI coordinate system, and the algorithms needed to depict the TCMS distribution as a pseudocolour contour map on the cortical surface. The methods are validated using TCMS data from the hand (thenar) and leg (tibialis muscle). The methods used correctly depict the expected motor representations of each of these areas and we therefore propose that this technique may be used as a functional imaging tool in the investigation of cortical function in both normals and patients. © 1997 Elsevier Science Ireland Ltd.

Keywords: TCMS; MRI; Co-registration; Rendering

1. Introduction

Trans-cranial magnetic stimulation (TCMS) allows the selective stimulation of different cortical areas, using a magnetic field pulse (Barker et al., 1985). This stimulation can be correlated with a measured external response, m, such as an evoked motor potential in a particular muscle group (Wasserman et al., 1992), or a change in detection thresholds for psychophysical stimuli (Beckers and Homberg, 1995; Beckers and Zeki, 1995). If the stimulator coil-set is moved systematically over a grid defined on the scalp, a topographic map of the distribution of m can be constructed (see Fig. 1). Given these external measurements we must then calculate which areas of the brain give rise to the response we have measured. This can be characterised as an inverse problem which has many similarities with the inversion of magnetoencephalographic (MEG) data to find the neuronal current distribution.

Suppose we define a function, $\mathbf{F}(\mathbf{r}_b)$ at each point in the brain, $\mathbf{r}_b$, which is only non-zero in those areas which are functionally correlated with the response. It is therefore the 'functional map' which we wish to determine and is a measure of the functional importance of a particular cortical area to the response we are measuring. We can also define a geometrical function, $\Phi_i(\mathbf{r}_b)$ (known as the lead field) which characterises the spatial variation of the magnetic stimulation at each point in the brain, when the coil is at grid position i. Then, the evoked response, m_i generated by stimulation at this grid point is:

$$m_i \propto \int_{Brain} \mathbf{F}(\mathbf{r}_b)\Phi_i(\mathbf{r}_b)\mathrm{d}v$$

Note that both $\mathbf{F}(\mathbf{r}_b)$ and $\Phi_i(\mathbf{r}_b)$ are vector functions, as it is likely that the relative orientation of the cortical neurons and the activation stimulus is important.

We can calculate $\Phi_i(\mathbf{r}_b)$ and we measure m_i, so this equation must be inverted to find the functional map $\mathbf{F}(\mathbf{r}_b)$. It is interesting to compare this equation with the general equation for the MEG forward problem (Hämäläinen et al., 1993):

$$m_i \propto \int_{Brain} \mathbf{J}(\mathbf{r}_b)\Phi_i(\mathbf{r}_b)\mathrm{d}v$$

In this case m_i is the measurement of the ith MEG detector coil, $\mathbf{J}(\mathbf{r}_b)$ is the current density in the brain at point $\mathbf{r}_b$, and $\Phi_i(\mathbf{r}_b)$ is the lead-field function of the coilset. Again, m_i is

* Corresponding author. Tel: +44 1784 443705; fax: +44 1784 434347; e-mail: k.singh@rhbnc.ac.uk

PII S0921-884X(97)96699-6

EEM 96699

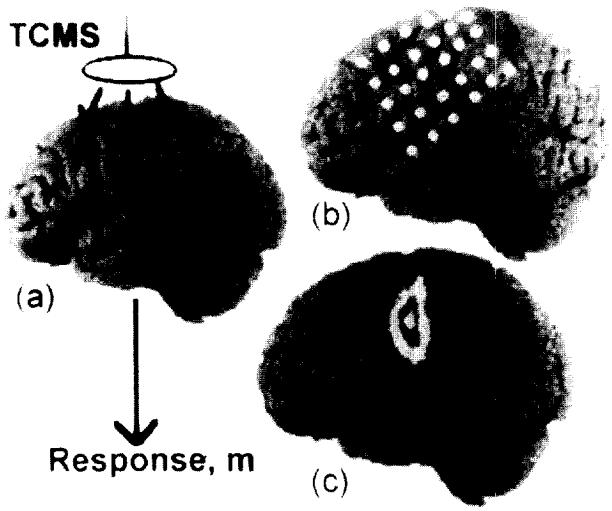

Fig. 1. Schematic showing the principle behind topographic mapping of TCMS. (a) A magnetic pulse in a particular portion of the brain elicits a measurable and quantifiable response m, somewhere in the body. The magnitude of m will vary with the position of the stimulator coil. By positioning the coil at several grid positions (b) a topographic map of m can be constructed (c).

measured and $\Phi_i(\mathbf{r}_b)$ is known, with $\mathbf{J}(\mathbf{r}_b)$ to be determined by inversion.

As the two equations are similar in form and are mediated by the same lead-field function, in principle the TCMS Inverse Problem could be solved using similar algorithms to those used in MEG. As with MEG there is a problem of non-uniqueness (i.e. there will a multiplicity of possible solutions for $\mathbf{F}(\mathbf{r}_b)$). For example, the form of the lead-field function is such that we cannot distinguish between a deep focal solution for $\mathbf{F}(\mathbf{r}_b)$ and a diffuse superficial one. As with MEG and electroencephalography (EEG), a solution can only be found by adopting an a-priori model for the form of $\mathbf{F}(\mathbf{r}_b)$. For example, the assumption that $\mathbf{F}(\mathbf{r}_b)$ is non-zero only in a single small area of the brain is directly equivalent to the single equivalent current dipole model in MEG/EEG.

In practice there are two additional problems in finding a true solution to the TCMS Inverse Problem. Firstly, in the above analysis we have assumed a linear transfer function between the magnitude of the field pulse and the measured response, m_i. In practice, the precise relationship between the intensity of stimulation and the evoked motor activity is not always known and may vary between different cortical areas. Although it is possible to numerically calculate the electric field evoked by magnetic stimulation at each point in the brain, the relationship between this electric field and the trans-membrane potential induced in the cortical neurons is not clear (Roth et al., 1991). This is in contrast to the MEG forward problem described above, where the linear relationship between the neuronal current and the measured signal is a fundamental relationship arising from the theory of electromagnetism.

Secondly, the physical size of most TCMS coilsets is large compared to MEG detectors. This results in lead-field functions which are spatially extended and hence reduces the spatial resolution achievable in the determination of the functional map.

In this paper we do not explicitly invert the integral equation to find a solution to the $\mathbf{F}(\mathbf{r}_b)$ distribution. Instead, we show how the measurements may be mapped onto the cortical surface to yield information about the topographic distribution of the measurement space, m_i. However, as it is considered likely that the most of the cortical activation is within 15–20 mm of the cortical surface (Rudiak and Marg, 1994) and the figure-of-eight coilsets used in this work produce activation in a well focused region directly below the centre of the coilset (Cohen et al., 1990; Roth et al., 1991), these topographic maps will be a first approximation to a solution for $\mathbf{F}(\mathbf{r}_b)$, i.e. the form of $\mathbf{F}(\mathbf{r}_b)$ is assumed to be a two-dimensional distribution on the surface of the cortex. A similar approximation is made for MEG measurement systems utilising figure-of-eight gradiometer designs (Hämäläinen, 1989).

The cortical surface representation to be used is a 3-dimensional rendered image of the brain, derived from magnetic resonance imaging (MRI) scans. In order to perform the topographic mapping, the functional data must first be co-registered with the co-ordinate system of the MRI scan, and we use a bite-bar-based method (Singh et al., 1997). Then, the surface rendered view of the brain must be generated and finally the data must be contour mapped onto this surface. In this paper we shall describe in detail the algorithms used to perform this procedure and we illustrate the proposed technique using TCM stimulation of the region of motor cortex representing the thenar area of the hand, and the tibial region of the leg.

2. Methods and materials

2.1. TCMS procedure

TCMS was performed using a commercial stimulator (Magstim 200, Magstim Ltd., UK) which has a figure-of-eight coil with loop diameters of 70 mm. This system was used to provide focal stimulation of up to 2.2 Tesla.

The experimental subject wore a closely fitting skullcap. Over each side of the head, a 14 cm × 10 cm grid, with points spaced antero-posteriorly by 2 cm and medio-laterally by 1 cm, was defined and each point marked on the skullcap. The position of the grid was such that its most medial and posterior corner was 2 cm posterior to the vertex.

During the experiment, the TCMS coil was placed so that junction of the coilset was directly above one of the grid points (e.g. point i). Thus, the maximum activation of the cortical surface was directly below the grid point (Cohen et al., 1990). As cortical excitation produced by magnetic stimulation is dependent upon coil orientation relative to the scalp surface, the figure-of -eight coil was always placed at a

fixed angle, tangential to the scalp surface, with the long axis of the coilset at 45° to the local vertical.

Surface electrodes were applied over the contralateral thenar eminence of the hand, in line with the 1st metacarpal bone. For one subject, data were also collected with the surface electrode over the contralateral tibialis anterior muscle. In a brief initial pilot study, each grid point was stimulated with an intensity of 60–80% of the maximum stimulator output to find the grid point which elicited maximum thenar or tibial response. Once the site of maximum response was identified, the coilset was re-positioned over this point and discharged at a sub-threshold of 20% stimulator output. This intensity was increased in 5% steps until an intensity was found which evoked quantifiable EMG responses of greater than 30 μV in 50% of 6 repeated measures. This intensity is then defined as the threshold stimulus intensity (Rossini et al., 1994).

The main stimulation phase of the experiment was then carried out with the coil moved in a pre-determined random order to each point in the grid and a pulse of 20% (of stimulator output) above threshold was delivered. 3 stimulations were made, separated by 15 s, and the mean response value was then calculated. In the distal muscle groups studied here, 3 repetitions were found to give an acceptable degree of repeatability for mapping purposes, without making the studies unduly lengthy and fatiguing for the subject. However, for more proximal muscle groups, a greater number of repetitions are required (Brasil-Neto et al., 1992), resulting in a more lengthy mapping procedure. In this paper we present results from 3 subjects, QA, SH and GT.

2.2. Co-registration with MRI

After the TCMS experiment, the 3-dimensional co-ordinates of each of the grid points was measured using a digitising pen system (Polhemus Isotrak system, Kaiser Aerospace Inc.). This system gives the x, y and z coordinates of each grid point, referenced to a radio-frequency magnetic field transmitter. The procedure was carried out with the subject biting on a custom-made dental bite-bar (Singh et al., 1997) which keeps the head fixed with respect to the Polhemus transmitter. In addition to the TCMS grid points, 6 specially machined holes in the bite-bar are also digitised. These extra fiducial marker points are used in the co-registration process.

The subjects were given a high resolution MRI scan using a 1.0 Tesla Siemens Magnetom system. For satisfactory rendering results we have found that a slice resolution of 1 mm × 1 mm with an inter-slice gap of no more than 1.5 mm is desirable. The scan is a T1 image designed to give good anatomical definition. During the MR scan, the subject wore the same dental bite-bite bar used in the TCMS grid point digitisation. The 6 holes in the bite-bar were filled with vitamin oil which is visible on the MR scans as a high contrast marker, and thus allows the identification of each of the 6 fiducial points in the MR co-ordinate system.

We now have 3-dimensional coordinates for each of the 6 fiducial markers in both the TCMS and MRI coordinate systems. This allows us to calculate a coordinate transform which will transform any point in the MRI system into the TCMS system (or vice-versa). Any such transform can be defined by a 3 × 3 rotation/scaling matrix A and a translation vector, r_0, and can be expressed as the following equation:

$$r^{\mathrm{TCMS}} = A\left(r^{\mathrm{mri}} + r_0\right)$$

We solve this equation by a least squares minimisation, using the Powell algorithm (Press et al., 1989), of the chi-square value:

$$\chi^2 = \sum_{i=1}^{6} \left(r_i^{\mathrm{TCMS}} - A(r_i^{\mathrm{mri}} + r_0)\right)^2$$

with respect to the elements of A and r_0. Once these parameters have been determined, we can now transform each of the TCMS grid points so that they can be represented on the MRI scans. The accuracy of this method of co-registration has been evaluated (Singh et al., 1997) and depending on the cortical region of interest, co-registration accuracies of a few mm are attainable. Another advantage of the bite-bar co-registration method is that the MRI need only be carried out once for each subject. Then, any experiment that is carried out at a later date using TCMS (or any other functional imaging technique) may be co-registered with the original MRI set, as long as the same bite-bar is used and the same fiducial points are digitised. Note that the bite-bar need only be used for the relatively brief Polhemus phase of the experiment, not for the actual TCMS measurement period.

2.3. Extraction of grey and white matter

We wish to render the cortical surface of the brain. In order to do this, we must first remove all extraneous structures (skull, scalp etc.) from the MR scans. We use a semi-automatic procedure which seems to yield satisfactory results with a moderate amount of operator intervention.

The software sequentially displays each slice of the MR volume set. Under operator supervision a rectangular region is defined which just encloses the brain and all pixels outside this region are set to zero. Then, all pixels which have grey-scale values outside the normal range for grey or white matter are also set to zero. In most cases this is sufficient to separate the brain from the skull/scalp. The operator then selects a point in the brain and a floodfill operation occurs from this point so that all points which are connected to the selected point are filled with a chosen colour (e.g. green). In some cases this fill operation erroneously 'leaks' over into unwanted parts of the image via small 'bridges' which survived the thresholding operation. The operator can interactively remove these until only the wanted part of the slice is

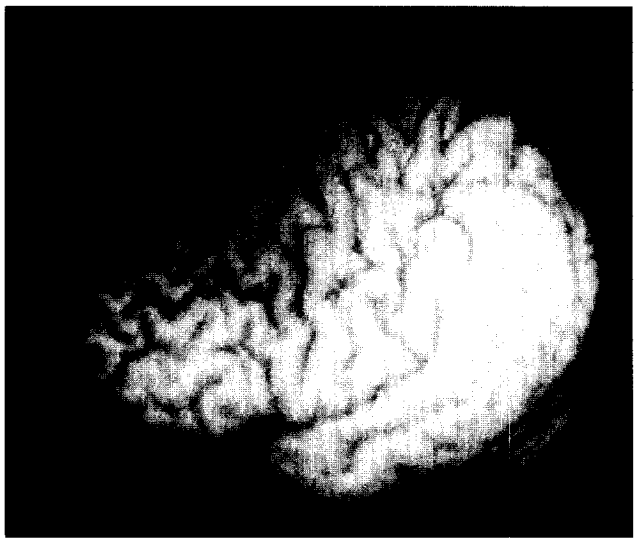

Fig. 2. A surface rendered image of the cortical surface of the brain. The image is generated by first removing the skull and scalp from the raw MRI dataset and then rendering the image using an integrated shading method (Bomans et al., 1990).

coloured green. The green image is used in a Boolean AND operation on the original image to yield a new image of the slice, containing only the brain.

The result of this procedure is another set of MRI scans which only contain voxels representing the brain. The number and geometry of these scans is identical to the 'raw' MR scans and so the coordinate transform defined in the previous section is still valid. This procedure for brain extraction is a relatively simple algorithm compared to more automatic ones which utilise spatial filters such as erosion and dilation (Wieringa, 1993), but we have found it to be a robust procedure which yields excellent results.

2.4. Surface rendering of the brain

To generate a surface rendered view of the extracted MRI brain volume, we use an integrated shading algorithm (Bomans et al., 1990). A view plane is set up outside the brain which can be in any position and orientation with respect to the centre of the brain. Simulated 'rays' are cast from each pixel in this view plane and those which do not intersect the brain are set to black. If a ray does 'hit' the cortical surface then we could simply colour the pixel with the greyscale of the MRI voxel that has been hit. However, such an image is dominated by noise and surface structures such as blood vessels. A much cleaner and more appropriate image results if we allow the ray to traverse into the brain by 5–10 voxels and integrate these voxels to provide a greyscale value. Further enhancements can be made by optimising the contrast and using depth shading so that parts of the brain furthest from the view plane are slightly darker than those nearest the observer. Fig. 2 shows a typical result.

Note that an image of the surface of the head can be generated in a similar way by rendering a view of the original MRI set (before brain extraction). Best results are achieved by simply using depth shading, without integrated shading.

2.5. Constructing a mapping surface

The procedure outlined above generates good quality surface rendered views of the brain in any orientation and position. Topographic mapping onto this surface view is not a trivial process as no actual parametric surface is generated. We could preferentially colour code each pixel as we generate the surface rendered view, using the TCMS data. However, this would be computationally intensive and would require the recalculation of the 3D cortical surface if, for example, we changed either the mapping parameters or the TCMS dataset. We believe a better approach is to generate a smooth surface representation of the surface of the brain which can be quickly rendered and rotated to any viewing position or orientation. Mapping onto this surface will be relatively straightforward and the TCMS dataset and mapping parameters (smoothing etc.) can be changed interactively.

The first stage in generating a mapping surface is to extract a set of boundary points from each slice in the

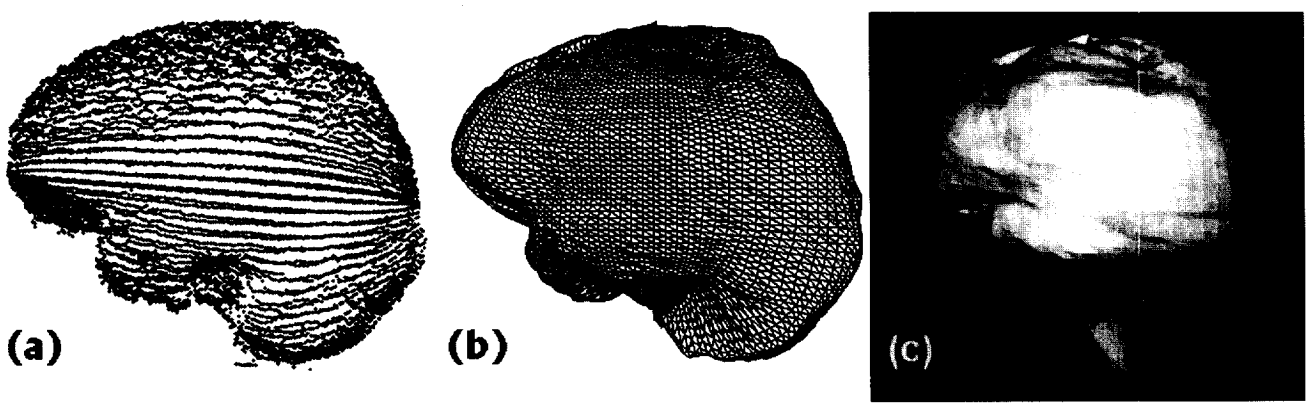

Fig. 3. An example of generating a parametric surface for contour mapping. (a) The 'cloud' of surface points extracted from the MRI scans of the brain. (b) The resultant surface, composed of triangular elements. In (c) the surface is rendered using a light shading model.

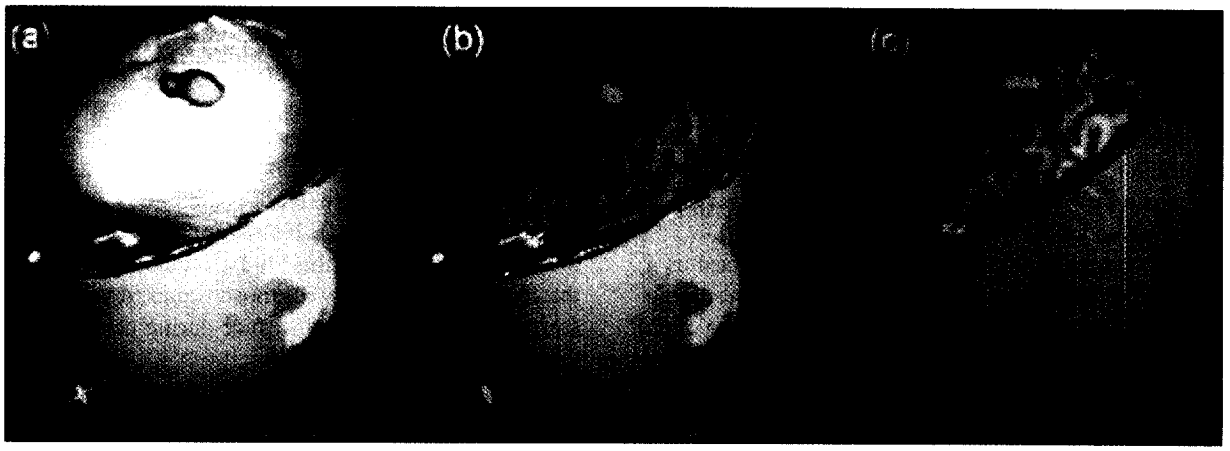

Fig. 4. Topographic mapping of TCMS data of the response at the right hand (thenar) onto a smooth surface representation (a) of the brain of subject QA. The coloured contour map can then be transferred onto a surface-rendered brain image (b) generated in the same position and orientation as the smooth mapping surface. In (c) the response at the thenar for subject SH is shown.

brain-extracted MRI set described above. The software does this automatically by firing an imaginary ray from the centre of the brain in each MRI slice and a boundary point is defined when this ray exits the brain. Rays are spaced at equal angular intervals and typically 75 points are defined on the boundary of each slice.

This procedure generates a 'cloud' of points in 3D space covering the surface of the brain (see Fig. 3a) which must be converted into a smooth surface. A convenient representation of such a surface is a set of triangles (Burger and Gillies, 1989). This set is easily generated by defining the vertices of each triangle to be adjacent triplets of points in the cloud. Often a rather uneven surface is generated by this method and smoothing of the triangle set is carried out.

In order to display the surface, each triangle is rendered onto the screen using a hidden surface removal algorithm utilising depth sorting (Burger and Gillies, 1989). Triangles facing away from the observer are also assumed to be invisible. Fig. 3b. shows a wireframe representation of the model. Alternatively, the greyscale value for each triangle can be calculated using a light shading model (Burger and Gillies, 1989). The parameters of the shading model can be varied, if desired, to give different appearances to the model (Fig. 3c).

The surface representation need only be generated once, and can then be rapidly displayed in any orientation under interactive control from the operator. It provides a substrate onto which any function can be topographically mapped.

2.6. Mapping of TCMS data onto the parametric surface

The mapping surface constructed in the previous section can be transformed into the TCMS coordinate system using the transformation parameters estimated in the co-registration procedure. Each of the TCMS stimulation points can then be projected onto the parametric surface at the nearest surface triangle to that grid point. With the figure-of-eight TCMS coilset (Cohen et al., 1990) used in this paper, the

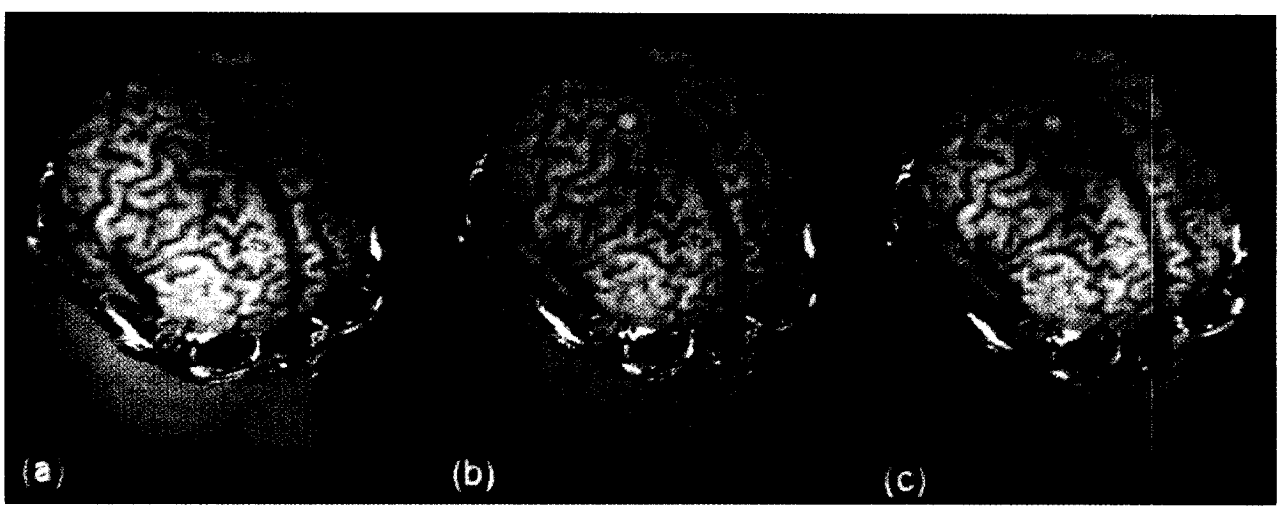

Fig. 5. Topographic mapping of TCMS data from subject GT. In (a) the response at the left thenar (hand) is shown, in (b) the response at the left tibial muscle of the leg and in (c) both responses are combined to demonstrate the separation of motor function on the pre-central gyrus.

nearest surface triangle on the brain is equivalent to the point where the lead-field function, $\Phi_i(\mathbf{r}_b)$, has its maximum magnitude. We now have a sparsely mapped function on the cortical surface. Using interpolation and smoothing, the function can be extended to the whole of the surface to form a smooth map. An appropriate choice of the smoothing parameters can be made by reference to the spatial variation of the $\Phi_i(\mathbf{r}_b)$ function.

The smoothed map is then displayed on the surface as a pseudo-colour representation with dark reds representing weak intensity, and orange and yellows representing high intensity. A threshold can be set such that the original grey-scale value of the surface shows through when the TCMS function is weak. Fig. 4a shows an example of such a map. Again, the model and map can be rotated and redisplayed rapidly.

2.7. Mapping onto the cortical surface image

Once the operator is satisfied with the view of the TCMS topographic map on the smooth surface model (Fig. 4a), the integrated cortical surface image can be generated in the same orientation and position (Fig. 4b). The contour map can then be transferred over onto the brain surface by simply copying the pseudo-colour pixels from one image to another. In this example, dithering has been used to give a 'transparent' effect.

3. Results

Figs. 4 and 5 show the mapping of thenar response data onto surface rendered MRI data for each of the 3 subjects, QA, SH and GT. In all cases the thenar representation consists of a single, well circumscribed region of primary motor cortex. In the case of GT the tibial response is shown together with the thenar response. The locations of the highlighted regions are, as expected, in the primary motor area along the pre-central gyrus. The spatial relationship of the hand and leg responses is as predicted from the classical homuncular model of sensory-motor cortex.

4. Discussion

We have shown how the topographic mapping of TCMS data onto surface-rendered views of the cortex, extracted from MRI data, can yield useful information about the functional organisation of the brain and we have given a detailed description of the algorithms used to generate these representations. The experimental results presented here validate the technique by showing how the known functional organisation of the motor representation of the hand and leg is correctly recovered.

With TCMS, we cannot be sure that evoked muscle activity results from direct stimulation of primary functional areas rather than, for example, depolarisation of projection fibres or cortico-cortico connections. This is most problematical for mapping of lower-limb motor cortex as the cortical representation is near the inter-hemispheric fissure, with its high density of cortical connections. This indeterminacy is common to all non-invasive functional imaging techniques (for example, there is ambiguity in the origin of EEG and MEG signals). However, it is reassuring to note that all areas found in this study, including the muscles of the leg, are consistent with those found in direct electrical stimulation of the cortical surface during neurosurgery (e.g. Penfield and Boldrey, 1937).

This topographic mapping method is an intermediate step between simply drawing a symbol on the cortical surface at the point where stimulation elicits the maximum response (Wasserman et al., 1996), and an attempt to calculate the true source localisation by inversion. The approach advocated here has the advantage that as well as showing the point of maximal activation, it gives a measure of the spatial extent of the cortical region implicated in the response.

These methods have been used in a clinical study of the cortical representation of swallowing musculature in normals and stroke patients (Hamdy et al., 1996). In addition, the co-registration and rendering techniques described here can be used to represent functional localisations from other imaging modalities such as MEG (Anderson et al., 1996), EEG and functional MRI.

Because of the inherent ambiguities in all functional imaging tools, a multimodality approach to functional imaging is necessary, with as many tools as possible brought to bear on the specific cortical function that is of interest. As we have demonstrated here, TCMS can be thought of as an additional functional imaging tool and can potentially be used as part of such a multimodal investigation in which the various functional data are co-registered and mapped onto a common MRI representation.

Acknowledgements

The authors would like to thank Mr. P. Furlong and Prof. G.F.A. Harding of Aston University, UK, for their assistance.

References

Anderson, S.J., Holliday, I.E, Singh, K.D. and Harding, G.F.A. Localisation and functional analysis of human cortical area MT (V5) using magneto-encephalography. Proc. R. Soc. Lond. Ser. B, 1996, 263: 423–431.

Barker, A.T., Jalinous, R. and Freestone, I.L. Non-invasive magnetic stimulation of the human motor cortex. Lancet, 1985, 1: 1106–1107.

Beckers, G. and Homberg, V. Cerebral visual motion blindness: transitory akinetoposia induced by transcranial magnetic stimulation of human area V5. Proc. R. Soc. Lond. Ser. B, 1995, 249: 173–178.

Beckers, G. and Zeki, S. The consequences of inactivating areas V1 and V5 on visual motion perception. Brain, 1995, 118(P + 1): 49–60.

Bomans, M, Hohne, K.H., Tiede, U. and Riemer, M. 3-D segmentation of MR images of the head for 3-D display. IEEE Trans. Med. Imaging, 1990, 2: 177–183.

Brasil-Neto, J.P., McShane, L.M., Fuhr, P., Hallett, M. and Cohen, L.G. Topographic mapping of the human motor cortex with magnetic stimulation: factors affecting accuracy and reproducibility. Electroenceph. clin. Neurophysiol., 1992, 85: 9–16.

Burger, P. and Gillies, D. Interactive Computer Graphics: Functional, Procedural and Device Level Methods. Addison-Wesley, 1989.

Cohen, L.G., Roth, B.J., Nilsson, J., Dang, N., Panizza, M., Bandinelli, S., Friauf, W. and Hallett, M.. Effects of coil design on delivery of focal magnetic stimulation: technical considerations. Electroenceph. clin. Neurophysiol., 1990, 75: 350–357.

Hämäläinen, M.S. A 24-channel planar gradiometer: system design and analysis of neuromagnetic data. In: S.J. Williamson, M. Hoke, G. Stroink and M. Kotani (Eds.), Advances in Biomagnetism. Plenum Press, New York, 1989, pp. 639–644.

Hämäläinen, M., Hari, R., Ilmoniemi, R., Knuutila, J. and Lounasmaa, O. Magnetoencephalography: theory, instrumentation and applications to noninvasive studies of the working human brain. Rev. Mod. Phys., 1993, 65: 413–496.

Hamdy, S., Aziz, Q., Rothwell, J.C., Singh, K.D., Barlow, J., Hughes, D., Tallis, R.C. and Thompson, D.G. The cortical topography of human swallowing musculature in health and disease. Nature Med., 1996, 2(11): 1217–1224.

Penfield, W. and Boldrey, E. Somatic motor and sensory representations in the cerebral cortex of man as studied by electrical stimulation. Brain, 1937, 60: 389–443.

Press, W.H., Flannery, B.P., Teukolsky, S.A. and Vetterling, W.T. Numerical Recipes in C. Cambridge University Press, Cambridge, 1989.

Rossini, P.M., Barker, A.T., Berardelli, A., Caramia, M.D., Caruso G., Cracco, R.Q., Dimitrijevic, M.R., Hallett, M., Katayama Y., Lucking, C.H., Denoordhout, A.L.M., Marsden, C.D., Murray, N.M.F., Rothwell, J.C., Swash, M. and Tomberg, C. Non-invasive electrical and magnetic stimulation of the brain, spinal cord and roots: basic principle and procedures for routine clinical application. Report of an IFCN committee. Electroenceph. clin. Neurophysiol., 1994, 91: 79–92.

Roth, B.J., Saypol, J.M., Hallett, M. and Cohen, L.G. A theoretical calculation of the electric field induced in the cortex during magnetic stimulation. Electroenceph. clin. Neurophysiol., 1991, 81: 47–56.

Rudiak, D. and Marg, E. Finding the depth of magnetic brain stimulation: a re-evaluation. Electroenceph. clin. Neurophysiol., 1994, 93: 358–371.

Singh, K.D., Holliday, I.E., Furlong, P.L. and Harding, G.F.A. A comparison of bite-bar and head-based MRI/MEG co-registration strategies using Monte Carlo simulation. Electroenceph. clin. Neurophysiol., 1997, 102: 81–85.

Wasserman, E.M., McShane, L.M., Hallet, M. and Cohen, L.G. Noninvasive mapping of muscle representation in the human motor cortex. Electroenceph. clin. Neurophysiol., 1992, 85: 1–8.

Wasserman, E.M., Wang, B.S., Zeffiro, T.A., Sadato, N., Pascual-Leone, A., Toro, C. and Hallett, M. Locating the motor cortex on the MRI with Transcranial Magnetic Stimulation and PET. Neuroimage, 1996, 3(1): 1–9.

Wieringa, H.J. MEG, EEG and the Integration with Magnetic Resonance Images. PhD Thesis, University of Twente, Enschede, The Netherlands, 1993.